3-2014

Design Considerations for Integral Abutment/ Jointless Bridges in the USA

Ralph G. Oesterle
Building and Environmental Consultants, roesterle@building-investigations.com

Habib Tabatabai
University of Wisconsin - Milwaukee, ht@uwm.edu

Cover page

Title: **Design Considerations for Integral Abutment/ Jointless Bridges in the USA**

Authors: Ralph G. Oesterle
Principal
Building and Environmental Consultants (BEC)
1019 Airpark Drive
Sugar Grove, IL 60554, USA
Phone: (630) 556-4950
Fax: (630) 556-9710
E-Mail: roesterle@building-investigations.com

Habib Tabatabai (Presenter and contact person)
Associate Professor
Department of Civil Engineering
University of Wisconsin-Milwaukee
3200 N Cramer Street
Milwaukee, WI 53211, USA
Phone: (414) 229-5166
Fax: (414) 229-6958
E-Mail: ht@uwm.edu

Proceedings of the 1st International Workshop on Integral Abutment/Jointless Bridges, Fuzhou University, China, March 2014, pp. 71-101

Design Considerations for Integral Abutment/ Jointless Bridges in the USA

Ralph G. Oesterle and Habib Tabatabai

ABSTRACT

This paper summarizes results of a major study on jointless bridges sponsored by the U.S. Federal Highway Administration. This study included extensive laboratory and field experiments as well as detailed analytical studies. A set of design recommendations were provided. Jointless bridges have reduced maintenance, improved riding quality, lower impact loads, reduced snowplow damage, and structural continuity for live load and seismic resistance. However, the thermal movements of the bridge and restraint forces from the abutments and piers must be considered and accommodated. The general design philosophy is to build flexibility into the support structures to the extent feasible while providing sufficient strength for restraint forces that cannot be completely eliminated. The experimental phase of the research addressed thermal movements and stresses; creep and shrinkage movements, including the effects of exposure to the outside environment; and pile behavior. The overall analytical program consisted of studies on abutment soil-structure interaction, pier behavior, longitudinal bridge movement, secondary continuity forces, skewed bridge behavior, and construction sequences. In some cases, the research demonstrates that existing design procedures and engineering data can be used to adequately quantify the structural response and design forces for the structure. In other cases, the results of more complex analyses were used to develop simplified design relationships and procedures.

Ralph G. Oesterle, Principal, Building & Environmental Consultants, 1019 Airpark Drive, Sugar Grove, IL 60554, USA
Habib Tabatabai, Associate Professor, University of Wisconsin-Milwaukee, 3200 N Cramer St., Milwaukee, WI 53211, USA

BACKGROUND

Over the years, many types of expansion joints, expansion bearings, and other structural release mechanisms have been used on long, multi-span highway bridges to accommodate thermal movements. The desirable characteristics of an expansion joint are watertightness, smooth rideability, low noise level, wear resistance, and resistance to damage caused by snowplow blades. The actual performances of many joint systems, however, are disappointing. When subjected to traffic and bridge movement, they typically fail in one or more important aspects, notably watertightness. [3]

Jointless bridges have the advantages of improved riding quality, lower impact loads, reduced snowplow damage, and structural continuity for live load and seismic resistance. On a jointless bridge, however, special considerations are required for movement and/or restraint stresses resulting from creep, shrinkage, and thermal strains in the design and detailing of the piers, abutments, and approach slabs. The general design philosophy is to build flexibility into the support structures to the extent feasible while providing sufficient strength for the restraint forces that cannot be completely eliminated.

The uncertainty and complexity in behavior and design have made some States and designers reluctant to use the jointless concept and may have led to some inefficiency in design by those States and designers that do use it. The design and construction of jointless bridges started with relatively short structures having only a few spans. The success of these structures in eliminating joints has resulted in the use of jointless bridges for increasingly longer structures. While these structures have generally performed well, their design and construction have been based principally on experience obtained over the years. Where problems have occurred, the causes have been identified and the procedures improved for the next structure. The design of jointless bridges has, for the most part, been based on empirical rules rather than rigorous engineering principles.

Major questions identified in this study included the effect of annual temperature variations, including the influence of internal restraint and thermal mass on temperature movement; effect of diurnal temperature variations; effective coefficients of thermal expansion; effects of creep and shrinkage on thermal expansion; foundation stiffness, particularly the relationship between passive earth pressure and abutment movement and the capacity of abutment piles to accommodate the movement; pier stiffness and load transfer to the piers; and response of skewed jointless bridges to annual and diurnal temperature variations.

OBJECTIVES AND SCOPE

The overall objectives of this research effort were to develop a greatly expanded knowledge of the behavior of jointless bridges, provide a scientific basis for design, and make design recommendations. This research work consisted of an experimental program and an analytical program. The scope of work included jointless bridges with composite steel, prestressed concrete and reinforced concrete beams subjected to gravity loads combined with thermal loads, and the time-dependent effects of concrete creep and shrinkage.

The experimental work included material and girder component tests, including constructing and monitoring two full-scale, two-span continuous girders in an outdoor environment for a period of 20

months. The experimental work also included field surveys of 15 jointless bridges and field monitoring of a long, heavily skewed jointless bridge.[6] The analytical work included assessment of the interaction of jointless bridge superstructures with integral abutments and piers, and the effects of secondary continuity forces in combination with end-restraint forces.[7] Skew effects were included and retrofitting of existing jointed bridges to eliminate expansion joints was addressed. The field survey of jointless bridges also included curved bridges.

SUMMARY OF FINDINGS AND RECOMMENDATIONS

In this section, findings and recommendations related to various issues that were studied are summarized and discussed.

Abutment-Soil Interaction

The soil pressure and abutment movement data shown in figure 1, as developed by G.W. Clough and J.M. Duncan[5] and presented in the NCHRP Report 343,[8] represent a reasonable upper-bound to determine the portion of full passive Rankine pressure to be used as a design passive pressure at the expected maximum abutment movement.

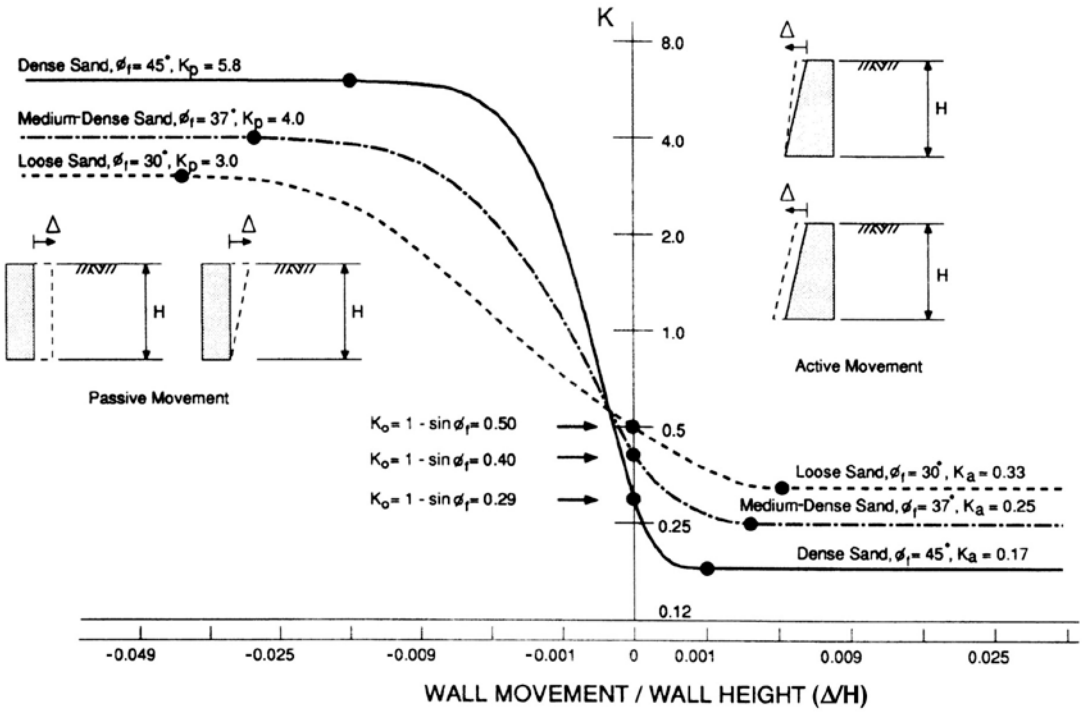

Figure 1. Relationship between abutment wall movement and earth pressure.[5,8]

The starting point for calculating maximum design passive pressure should conservatively be at the point of maximum contraction (from creep, shrinkage, and thermal strain) of the bridge superstructure. As contraction decreases the soil pressure to the minimum active pressure, the granular soil will follow the contacting abutment wall and re-compact. The re-compaction is

sufficient to shift the soil pressure and abutment movement curve so that passive pressure starts to build immediately upon thermal re-expansion.

There are opposing philosophies as to the degree of compaction in the backfill soil adjacent to the abutment. One concept is to use loose granular backfill to minimize passive pressure forces. The opposite concept is to use highly compacted backfill based on the observation of voids beneath the approach slab and settlement of the approach slab as a common problem with integral abutments. Tests on a large-scale abutment specimen[9] indicated that voids under the approach slabs develop as a result of contraction beyond the initial starting point, even with 97 percent relative compaction of the backfill adjacent to the abutment. Therefore, there does not appear to be an advantage to using high compaction. Also, a high degree of compaction is difficult to attain in the location adjacent to the abutment backwall.

Parametric computer analyses indicated that the passive pressure can be significantly decreased by using relatively uncompacted backfill and/or by increasing the horizontal length of the backfill zone behind the abutment. The calculated resultant passive soil reaction decreased by a factor of approximately 2.5, with a decrease in compaction from 90 percent to 80 percent. Also, with backfill at 80 percent compaction, the calculated resultant passive pressure decreased by a factor of approximately 2 when the slope of the backfill/in situ soil interface was changed from 45° to 30° (from horizontal). However, extending the backfill zone behind the abutment increases the length needed for the approach slab to span the backfill region and/or increases the settlement of the approach slab.

The shape of the pressure distribution is dependent on the rotation of the abutment wall, but typically includes a large increase in pressure at the base of the abutment. The concentration of pressure at the base increased with a decrease in rotation. The rotation of the abutment is dependent on the relative bending stiffness of the superstructure and the rotational stiffness of the soil/pile/abutment interaction. The pressure distribution shown in figure 2 is recommended for the design of stub abutments on piles. The pressure distribution shown in figure 3 is recommended for abutments on spread footings and the pressure distribution shown in figure 4 is recommended for full-height abutments.

Abutment Pile Capacity

The analytical approach selected for this study was based on the simplified model developed by Abendroth, et al.[1] Three criteria for determining abutment pile capacity were incorporated in this model. The first criterion was based on the geometric stability of the pile (elastic or inelastic buckling as a function of its vertical load and moment associated with lateral movement). The second criterion was related to material strength (usually governs in case of short or stubby piles). The third criterion was based on the rotational capacity of the pile (a ductility issue related to local hinging of the pile). The calculations associated with these three pile capacity criteria were based on an equivalent cantilever length of the pile. The equivalent cantilever length can be determined for either fixed or pinned conditions between the top of the pile and the bottom of the abutment.

The results of the parametric study are typically in the form of ultimate vertical load capacity versus lateral displacement of piles. A comparison was made with respect to the maximum assumed design vertical load obtained from AASHTO specifications,[28] considering no lateral

displacement and no soil data available. Examples of the results of analyses are shown in figures 5 through 7 for piles without overdrilled holes. The analyses were terminated either when the ductility limit was reached or when 100 mm (4 inches) of deflection were reached.

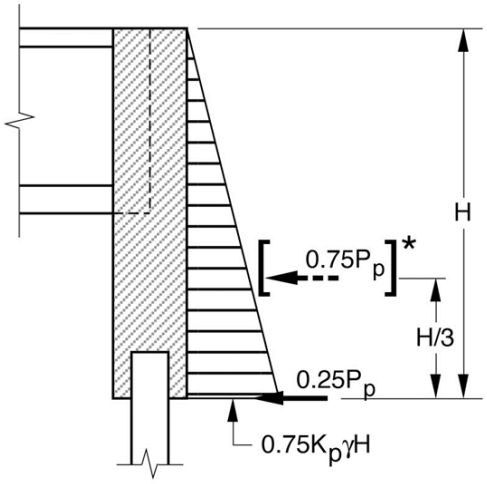

Figure 2. Proposed passive pressure distribution for design of integral stub abutments on piles

* Resultant of triangular distribution.
$P_p = ½ \gamma K_p H^2$
K_p = Passive pressure coefficient dependent on wall movement according to Clough and Duncan[5,8]

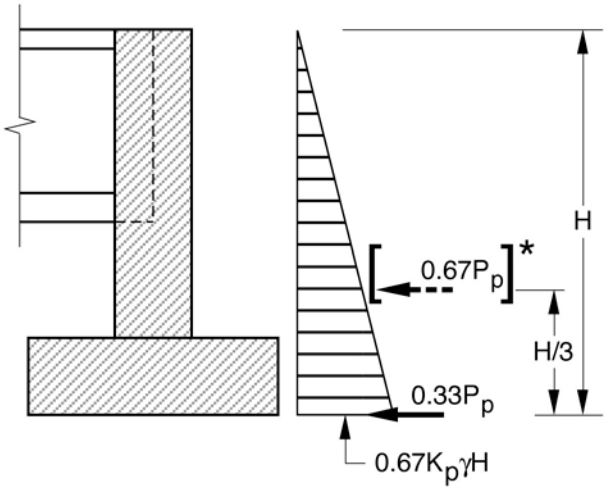

Figure 3. Proposed passive pressure distribution for design of integral stub abutments on spread footings

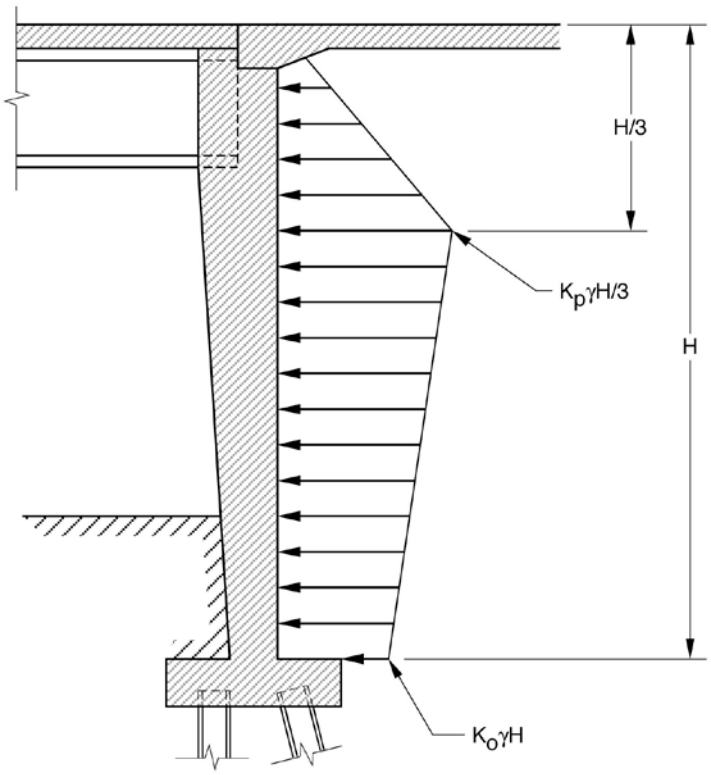

Figure 4. Proposed design envelope for full-height wall abutments based on passive and at-rest pressures

The data presented in figures 5 through 7 indicate that displacement capacities increase as soil stiffness decreases and as section size increases. The results of analyses for H-piles shown in figure 5 are based on weak-axis bending. Based on surveys of State DOT practices, it appears that many States prefer to orient H-piles for weak-axis bending under longitudinal movement, while other States prefer to use strong-axis bending. The rationale for weak-axis bending is that the flexibility of the pile is greater and the pile can therefore accommodate larger movements. However, the deformation capacity of the pile depends not only on the pile flexural stiffness, but on the combined pile and soil system stiffness. As the pile stiffness increases, the soil is affected to increasing depths. The effective cantilever length in bending therefore increases, tending to decrease the overall stiffness of the pile-soil system.

Analyses presented in the analytical report demonstrate that bending about the strong axis results in a larger displacement at first yield than bending about the weak axis.[7] For an HP10x42, the ratio of yield displacement for strong axis bending to yield displacement for weak-axis bending is approximately 1.7. It should be noted, however, that while strong-axis bending provides a larger displacement capacity, design forces for the pile-to-pile-cap connection are increased.

A summary of the findings and conclusions based on the analyses, literature review, and available test data for piles in integral abutments is as follows:

1. Vertical load capacity of an abutment pile is a function of the abutment's horizontal movement associated with bridge expansion or contraction. Vertical load capacities decrease when displacements increase.

2. Longitudinal displacement capacity increases as pile flexural stiffness increases and/or soil stiffness decreases. An increase in the ratio of pile stiffness to soil stiffness increases the effective cantilevered length of the pile. Therefore, the curvature demand associated with a particular lateral displacement is spread over a longer length and the ductility demand at that displacement is decreased. Based on these analyses, situating an H-pile for bending about the strong axis with abutment movement will allow larger displacement.

3. The steel H-pile test specimen demonstrated that slight local buckling of the flanges occurred during the tenth cycle of lateral displacement of the inflection point of ±61 mm (±2.4 inches). This displacement is the calculated deformation limit corresponding to the ductility criterion presented by Abendroth, et al.[1] Therefore, the test results indicated that the ductility criterion proposed by Abendroth et al., was appropriate. Also, the pile was able to sustain the load capacity through 50 cycles at this level of deformation without further deterioration of the section. Therefore, this criterion is recommended for the design of H-piles.

4. The analyses indicate that concrete-filled pipe piles have very large displacement capacities and generally lose a lower percentage of vertical load capacity at large displacements. Although no pipe piles were tested in the experimental program for this project, testing of concrete-filled steel tubular columns has shown a high degree of ductility with stable loops.[11] A conservative design approach would include limiting the maximum strain to 0.01 and the maximum aspect ratio of pile diameter to wall thickness to 39.

5. Analytical studies indicated that prestressed concrete piles would have significant displacement capacity if ductile behavior based on a maximum compressive strain limit is assumed. However, testing indicated that a prestressed concrete pile would suffer severe cracking and spalling if cycled at a deformation limit based on the ductility criteria used in the analytical study. Therefore, it is recommended that displacement limits for prestressed concrete piles be based on an allowable stress limitation as initially presented by Abendroth, et al.[2]

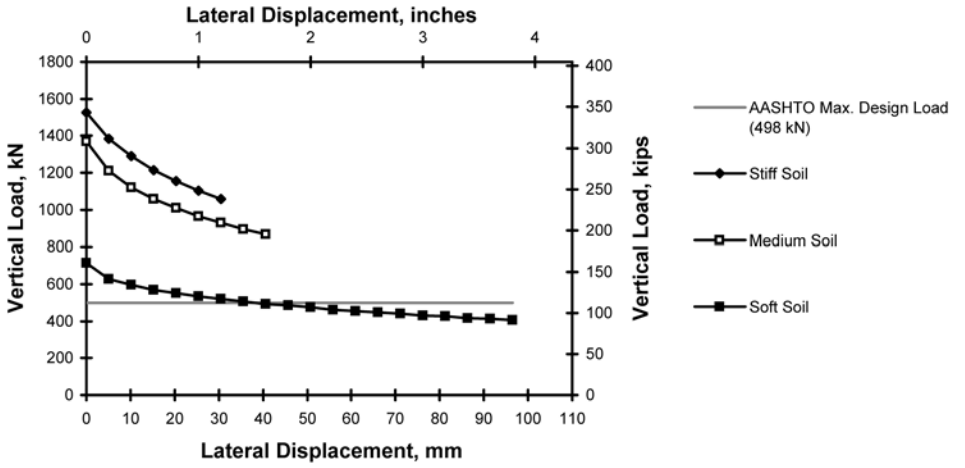

Figure 5(a). Ultimate load capacity for HP10x42 (without overdrilled holes)

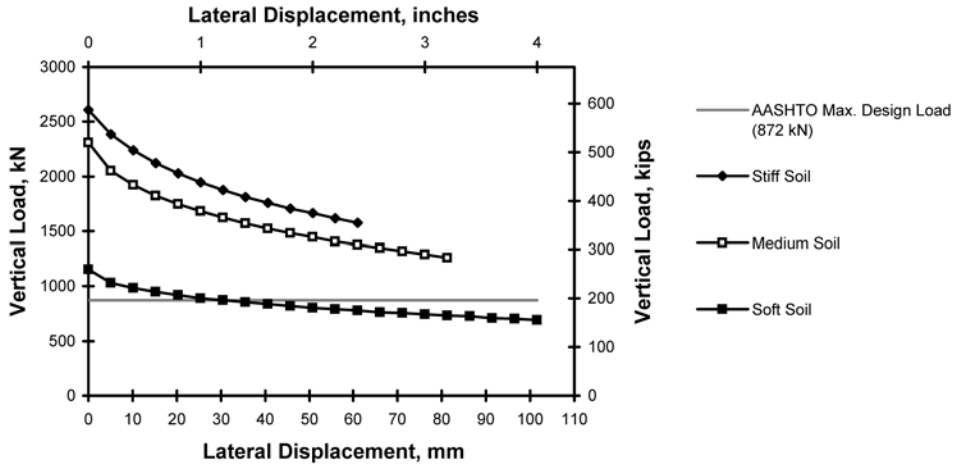

Figure 5(b). Ultimate load capacity for HP12x74 (without overdrilled holes)

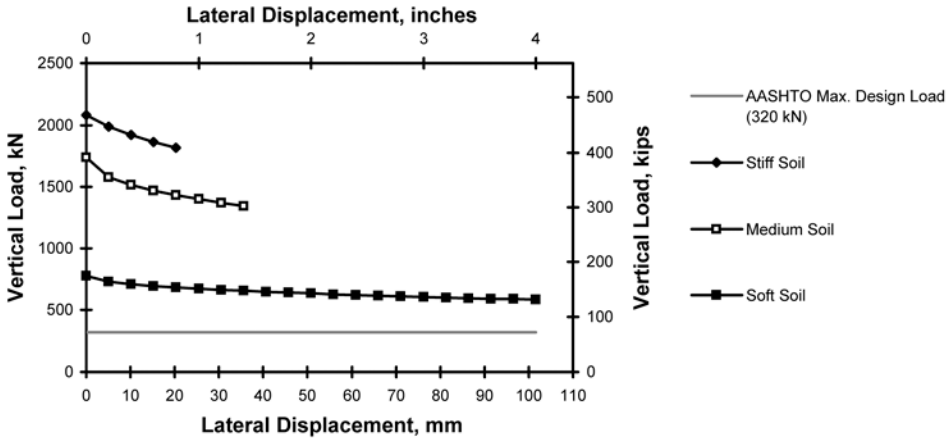

Figure 6(a). Ultimate load capacity for 406- by 406-mm (16- by 16-inch) prestressed concrete piles (without overdrilled holes).

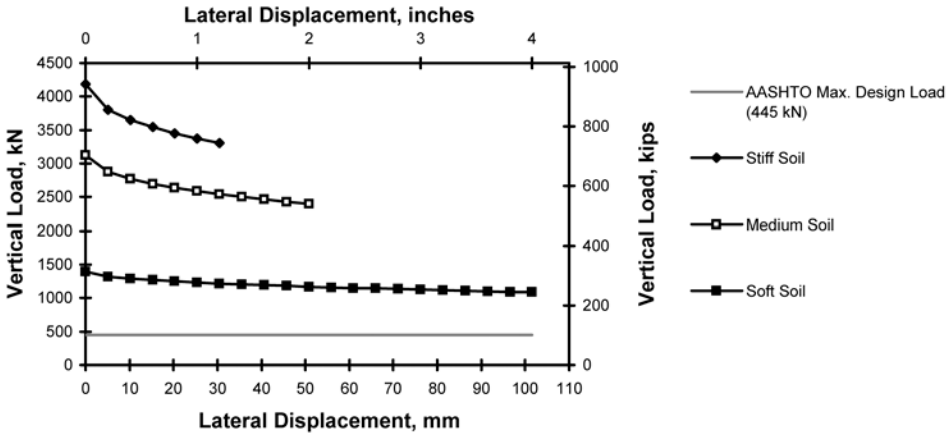

Figure 6(b). Ultimate load capacity for 610- by 610-mm (24- by 24-inch) prestressed concrete piles (without overdrilled holes).

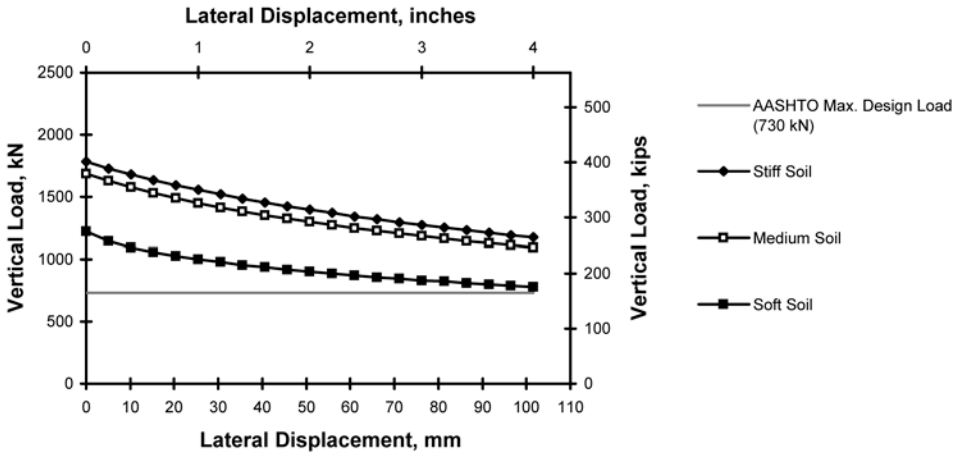

Figure 7(a). Ultimate load capacity for PP 12-3/4 (without overdrilled holes).

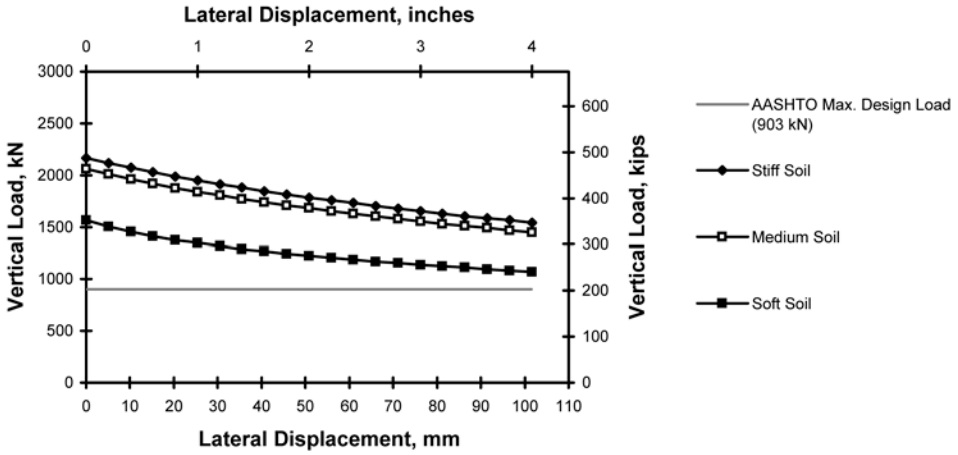

Figure 7(b). Ultimate load capacity for PP 16 (without overdrilled holes).

Effective Stiffness of Piers

There are two important factors in the effective response of piers to superstructure movement. The foundation response and nonlinear pier response (cracking, creep, and shrinkage) are considered and discussed below.

Foundation Response

The rotational stiffness of the foundation is an important factor in the response of piers to longitudinal deck movement. Foundation type and size, as well as soil stiffness, influence the rotational stiffness. The study indicated that the moment-rotation behavior was essentially linear and the rotational stiffnesses were consistent with a simplified analysis presented by J. Zederbaum.[12] Rotational stiffness, K_θ, using Zederbaum's approach, is based on the elastic

behavior of an ideal earth prism of a depth equal to one-third of the footing width, b, and can be determined as:

$$K_\theta = \frac{3E_s I_f}{b} \quad (1)$$

where,

E_s = modulus of elasticity of the soil

I_f = moment of inertia of the foundation base

b = footing width

The rotational stiffness of the pile foundation was based on an elastic approach presented by A.A. Witecki and V.K. Raina.[13]

Pier Response

The structural stiffness of the pier wall or columns is another important factor in estimating the restraining forces associated with longitudinal thermal movement of a bridge superstructure. Pier stiffness is a function of the slenderness ratio (i.e., height to thickness), concrete properties, applied vertical loads, inelastic behavior (i.e., creep and cracking of concrete), and the type of connection at the top of the pier (i.e., integral versus semi-integral or pinned piers). Integral piers will transfer both moment and shear forces at the top, whereas semi-integral piers transfer shear forces only.

Based on nonlinear parametric studies, the following relationship for the effective moment of inertia, I_e, for the pier is recommended:

$$I_e = \left(\frac{M_{cr}}{M_a}\right)^{1.25} I_g + \left[1 - \left(\frac{M_{cr}}{M_a}\right)^{1.25}\right] I_{cr} \leq I_g \quad (2)$$

in which,

M_a = calculated elastic moment based on assumed bridge movement

I_g = moment of inertia of gross concrete section about the centroidal axis, neglecting reinforcement

I_{cr} = moment of inertia of cracked section transformed to concrete

M_{cr} = cracking moment, can be calculated as follows:

$$M_{cr} = \left(\frac{P}{A} + f_r\right)\frac{I_g}{y} \quad (3)$$

where,

P = applied vertical load

A = cross-sectional area of concrete, neglecting reinforcement

y = half-depth of pier section

f_r = modulus of rupture of concrete

$= 0.62 \sqrt{f'_c}$ (MPa)

$= 7.5 \sqrt{f'_c}$ (lbf/inch^2)

f'_c = compressive strength of concrete

Results of the analyses for pier behavior indicate that foundation rotation contributed to a significant portion of the longitudinal movement at the top of the pier. For the range of parameters used in the study, the foundation rotation accounted for 20 percent to 79 percent of this movement.

The primary factors affecting the contribution of bending in the pier to the longitudinal movement at the top of the pier are the slenderness of the pier (height-to-thickness ratio) and cracking. Axial stress in the pier affects the cracking moment and, therefore, the effective stiffness. Concrete creep and the age of the concrete at loading had a relatively insignificant effect on the results.

Use of an integral pier with a moment connection between the pier cap and the superstructure will induce significantly higher restraint forces in the pier as compared to the case of semi-integral pier with a pinned connection. Since pier stiffness has a negligible effect on the total bridge movement, the stiffer connection does not decrease the expected movement at the top of the pier. Use of an integral pier eliminates the need for the elastomeric bearing pads and details to accommodate rotation between the pier cap and the superstructure. Also, integral piers eliminate the mass of the pier cap for seismic design and provide increased clearance. However, the details for a semi-integral pier are simple compared to detailing a moment connection at the top of the pier.

Expected Bridge Movement

The factors involved in predicting the expected bridge movements include an effective temperature range, including seasonal and diurnal components; coefficient of thermal expansion; creep, and shrinkage; and the restraint from piers and abutments. The overall variability of these factors causes uncertainty in the determination of bridge movements.

Effective Temperature Range

Emerson developed a relationship between instantaneous shade temperature and effective bridge temperature by first developing a relationship between the mean shade temperature and the effective bridge temperature.[3] Emerson then related the mean shade temperatures to the instantaneous shade temperatures based on meteorological data recorded throughout the United Kingdom. Imbsen applied and extended Emerson's approach to effective bridge temperatures in NCHRP Report 276.[4] To cover the larger range of minimum and maximum shade temperatures experienced within the United States, Imbsen extrapolated Emerson's mean and effective bridge temperature relationships. However, isotherms in NCHRP Report 276 only represent *normal* daily minimum and maximum values instead of the extreme values of shade temperatures.

The AASHTO LRFD Bridge Design Specifications (15) include two separate procedures for estimating bridge temperature ranges (Procedure A and B). This study considers Procedure A to be inadequate. Although Procedure B is closer to the actual bridge response than Procedure A, it is recommended that the temperature ranges be estimated using localized temperature data as proposed here. The following procedures are recommended to determine the range of the effective bridge temperatures:

1. Obtain the minimum and maximum shade temperatures from the ASHRAE weather data[14] for the State and weather stations nearest the bridge site, and interpolate as needed. An example of such data for major US cities is shown in table 1. The shade air temperatures given in table 1 should be adjusted at a rate of 1°C/100 m (1°F/200 ft) of elevation change.
2. Determine the solar zone for the bridge location using AASHTO LRFD specifications,[15] and the corresponding solar increment, $\Delta\overline{T}_{solar}$ from table 2.
3. Calculate minimum and maximum effective bridge temperatures from the following relationships:

For concrete bridges:

$$T_{min_{eff}} = 1.00\, T_{min_{shade}} + 5°C\ (9°F) \quad (4)$$

$$T_{max_{eff}} = 0.97\, T_{max_{shade}} - 2°C\ (3°F) + \Delta\overline{T}_{solar} \quad (5)$$

For composite steel bridges:

$$T_{min_{eff}} = 1.04\, T_{min_{shade}} + 2°C\ (3°F) \quad (6)$$

$$T_{max_{eff}} = 1.09\, T_{max_{shade}} - 0°C\ (3°F) + \Delta\overline{T}_{solar} \quad (7)$$

where,

$T_{min_{eff}}$ = minimum effective bridge temperature
$T_{max_{eff}}$ = maximum effective bridge temperature
$T_{min_{shade}}$ = minimum shade temperature from the weather data based on bridge location (table 1)
$T_{max_{shade}}$ = maximum shade temperature from the weather data based on bridge location (table 1)
$\Delta\overline{T}_{solar}$ = uniform temperature change from direct solar radiation based on girder type and bridge location (see table 2)

Table 1. Climatic conditions for major cities in the US

	Location					Shade Temperature		
	Latitude		Longitude		Elev.	Min.	Max.	Mean* Constr.
State & Station	°	lN	°	lW	m	°C	°C	°C
Birmingham, Alabama	33	34	86	45	189	-8	36	17
Anchorage, Alaska	61	10	150	1	35	-31	22	11
Phoenix, Arizona	33	26	112	1	339	-1	43	21
Los Angeles, California	33	56	118	24	30	5	28	17
Denver, Colorado	39	45	104	52	1610	-21	34	17
San Francisco, California	37	37	122	23	2	2	28	13
Miami, Florida	25	48	80	16	2	7	33	24
Atlanta, Georgia	33	39	84	26	308	-8	34	17
Washington, DC	38	51	77	2	4	-10	34	17
Seattle-Tacoma, Washington	47	27	122	18	122	-6	29	11
NYC, New York	40	39	73	47	4	-11	32	15
Boston, Massachusetts	42	22	71	2	5	-14	33	14
Chicago, O'Hare AP	41	59	87	54	201	-22	33	16
Minneapolis/St. Paul, MN	44	53	93	13	254	-27	33	17
St. Louis, Missouri	38	45	90	23	163	-17	36	18
Dallas, Texas	32	51	96	51	147	-8	39	19
Kansas City, Missouri	39	7	94	35	241	-17	37	18
Las Vegas, Nevada	36	5	115	10	664	-4	42	19
Charlotte, North Carolina	35	13	80	56	224	-8	35	16
Cincinnati, Ohio	39	9	84	31	231	-17	33	17
Baltimore, Maryland	39	11	76	40	45	-12	34	17

*Mean construction season shade air temperature [16].

Table 2. Solar increment values based on girder type and bridge location.

Zone	T_1	Concrete $\Delta\overline{T}$	Composite Steel $\Delta\overline{T}$
1	30°C	8°C	6°C
2	26°C	7°C	5°C
3	23°C	6°C	4°C
4	21°C	5°C	4°C

1°C = 1.8°F

Determination of Maximum Movements

In jointless bridges, it is important to estimate the maximum expansion and contraction at each end of a bridge to determine the longitudinal displacement expected for the abutment piles. It is also important to predict the movement at each pier and the joint width needed between the approach slab and the pavement. Another important movement is the maximum total thermal movement at each end resulting from the total effective temperature range. As discussed earlier, the starting point

to determine the maximum passive pressure should conservatively be at the maximum contraction. The maximum passive pressure is related to the end movement, with re-expansion for the full effective temperature range.

Calculation of the length change for a prestressed concrete bridge can be accomplished through use of typical design values for the coefficient of thermal expansion combined with creep and shrinkage strains from ACI 209.[17] However, the overall variability of these factors adds uncertainty to the calculated end movements. Although a coefficient of thermal expansion for concrete is typically assumed to be 9.9 to 10.9 millionths/°C (5.5 to 6.0 millionths/°F), it is known that this value can range from approximately 5.4 to 12.6 millionths/°C (3.0 to 7.0 millionths/°F).[18] Also, the variability of creep, shrinkage, and modulus of elasticity of concrete is known to be significant.[18] In addition, resistance to length change from abutments and piers, combined with the variability of the restraint (primarily caused by the variability of the soil), leads to unequal movement at each end of a bridge and uncertainty as to the magnitude of the movement at each end. Finally, the effective setting temperature of the bridge and the age of the prestressed concrete girders at completion of the superstructure are typically unknown, making the relative magnitude of expansion and contraction and the starting point for creep and shrinkage calculations uncertain.

To investigate the effects of the variability of the parameters and to provide guidance in formulating recommendations for design calculations, Monte Carlo studies were carried out. Two standard four-span bridge models were selected for these Monte Carlo studies. The first model was a prestressed concrete bridge that was modified to simulate various conditions. The second model included steel wide-flange stringers.

Table 3 presents the values of the magnification factors, referred to as Γ factors, for the various conditions based on the results of the Monte Carlo studies. These Γ factors are intended to modify the calculated values to account for uncertainty in the calculations. Case 1 includes magnification factors for the maximum expected movement from the assumed "as constructed" condition. A primary factor affecting the magnitude of these magnification factors is the uncertainty of the construction temperature. The Γ values for total movement account for uncertainty for the

Table 3. Values of Γ magnification factor.

Case No.	Design Condition	For Bridge Expansion		For Bridge Contraction	
		Total	End	Total	End
1(a)	Conventional Design of Prestressed Bridge	1.50	1.60	1.30	1.35
1(b)	Cast-in-Place Concrete Bridge	1.50	1.60	1.30	1.40
1(c)	Composite Steel Bridge	1.50	1.70	1.45	1.50
2	Re-expansion After Full Contraction	1.10	1.20	—	—

calculation of the overall change in the length of the bridge. However, because of uncertainty for the stiffness of the abutments and piers, the Γ's for the calculation of the movement at each end are somewhat larger. Case 2 addresses re-expansion from full contraction.

The following procedures are recommended to determine end movements in the longitudinal direction while accounting for the uncertainty of calculations. It is assumed that the date and temperature when the deck was cast are unknown and that no specific data on the material properties of the concrete are available other than 28-day compressive strength, f'_c. To determine the maximum end movements of a prestressed concrete bridge:

4. From table 1, determine the mean construction temperature for locations nearest the bridge, and interpolate to determine a mean construction temperature for the bridge location. Alternatively, determine a mean construction temperature from data for stations in the same part of the country with similar minimum and maximum shade temperatures.
5. To calculate end movements:
    a. Determine the minimum and maximum effective bridge temperatures from equations 4 and 5, respectively.
    b. Use typical design values of 10.8 millionths/°C (6.0 millionths/°F) for the coefficient of thermal expansion of concrete, values for creep and shrinkage from ACI 209,[16] and 4700 $\sqrt{f'_c}$, MPa (57,000 $\sqrt{f'_c}$, lbf/inch^2) for the modulus of elasticity of concrete.
    c. Use the procedure presented by Zederbaum[12] to determine the point of zero movement or the point of fixity within the bridge based on the stiffness of the piers and the abutments. The equivalent cantilever method can be used to estimate the lateral stiffness of the abutment piles. Since the responses of the piers and abutments are nonlinear, the stiffnesses should be based on a preliminary estimate of the end movements. It should be noted, however, that for a symmetrical bridge, the point of fixity would be at the longitudinal center of the bridge.
    d. The following equations are used to determine the strain values for a prestressed concrete bridge. Changes in length are determined by multiplying the strain by the total initial length.

$$\varepsilon_{th} = \alpha \, \Delta T \tag{8}$$

$$\varepsilon_{sh} = \varepsilon_{sh_{girder}} + \frac{\varepsilon_{sh_{deck}} - \varepsilon_{sh_{girder}}}{1 + \frac{(EA)_{girder}}{(EA)_{deck}}} \tag{9}$$

$$\varepsilon_{cr} = \varepsilon_{cr_{girder}} \left[\frac{1}{1 + \frac{(EA)_{girder}}{(EA)_{deck}}} \right] \quad (10)$$

$$\Delta\ell = \Gamma \varepsilon_{total} \ell \quad (11)$$

where,

ε_{th} = thermal strain
ε_{sh} = shrinkage strain
ε_{cr} = creep strain
α = coefficient of thermal expansion
E = modulus of elasticity
A = cross-sectional area
ℓ = length from calculated point of fixity to end of bridge. Note that, for a nonsymmetrical bridge, two different lengths are involved.
Γ = magnification factor to account for uncertainty

$$\varepsilon_{total} = \varepsilon_{th} - \varepsilon_{sh} - \varepsilon_{cr} \text{ for expansion} \quad (12)$$

$$\varepsilon_{total} = -\varepsilon_{th} - \varepsilon_{sh} - \varepsilon_{cr} \text{ for contraction} \quad (13)$$

$\Delta\ell$ = maximum end movement

6. Maximum expansion typically occurs shortly after construction. For this maximum expansion (Case 1(a) expansion in table 3), use the temperature differential between the maximum effective bridge temperature and the mean construction temperature for thermal expansion, and a time span equal to one-quarter of the construction season for creep and shrinkage contraction with the beams assumed to be 90 days old when the deck is cast. Based on the Monte Carlo studies, the calculated end movements should be increased by a Γ factor of 1.60 (see table 3) to account for the uncertainties with 98 percent confidence that the movement will be less than that calculated.

7. For maximum contraction after several years of service (Case 1(a) contraction in table 3), use the temperature differential between the minimum effective bridge temperature and the mean construction temperature for thermal contraction, and ultimate creep and shrinkage values with the beams assumed to be 10 days old at the time of casting of the deck. Based on the Monte Carlo studies, the calculated end movement should be increased by a Γ factor of 1.35 (see table 3) to account for uncertainties with 98 percent confidence that the movement will be less than that calculated.

8. For maximum thermal re-expansion from a starting point of full contraction (Case 2 in table 3), the full range of effective bridge temperatures should be used without any creep

or shrinkage movement. The resulting calculated end movements should be multiplied by a Γ factor of 1.20 (see table 3) to account for uncertainties in the calculation.

For reinforced concrete bridges, similar procedures can be used to determine the maximum expansion and contraction end movements. However, shortening caused by creep is not a factor. Calculated end movements for reinforced concrete bridges should be increased by the Γ factors for Case 1(b) of 1.60 for maximum expansion and 1.40 for maximum contraction. A Γ factor of 1.20 can be used for Case 2, maximum thermal re-expansion from a starting point of full contraction. Note that the magnitudes of the multipliers, Γ's, for Cases 1(a) and 1(b) are significantly larger than the multiplier, Γ, for Case 2 because of the uncertainty and variability of the construction temperature.

For composite steel bridges, the procedures used to estimate the maximum end movements are also similar to the procedures outlined above for the prestressed concrete bridges, except that a modulus of elasticity of 20×10^4 MPa (29×10^6 lbf/inch^2) and a coefficient of thermal expansion of 11.7 millionths/°C (6.5 millionths/°F) should be used for the steel girders. These values are recommended by AASHTO for structural steel. The results of the Monte Carlo study for composite steel bridges indicated that calculated end movements should be increased by the Γ factors for Case 1(c) of 1.70 for maximum expansion and 1.50 for maximum contraction. A Γ factor of 1.2 can be used for Case 2, maximum thermal re-expansion from a starting point of full contraction.

If sufficient information regarding the composition of the concrete is available to the designer, a more accurate value for the coefficient of thermal expansion of concrete can be obtained by using the Emanual and Hulsey model[20] to estimate the value of the coefficient of thermal expansion of concrete. Calculated end movements using the more accurate Emanual and Hulsey coefficient of thermal expansion of concrete should be increased by Γ factors of 2.05 for maximum expansion and 1.45 for maximum contraction. These Γ's are greater than the values calculated for the Case 1(a) or 1(b) condition. This is caused by the difference in calculating the design thermal movements rather than the variability of the predicted movements. The coefficient of thermal expansion design value of 10.8 millionths/°C (6.0 millionths/°F) recommended by AASHTO and used for Cases 1(a) and 1(b) is conservatively high when compared to the average of the data base.[7] The average coefficient of thermal expansion for concrete in the data base used in this study[7] is 8.8 millionths/°C (4.9 millionths/°F). Therefore, the conventional design calculated value of movement already includes some margin of safety.

Note that when using the Emanual and Hulsey model[20] to estimate α, the concrete for the deck slab is commonly different than the concrete for the beam. Therefore, an effective coefficient of thermal expansion, α_e, for the composite section can be calculated as:

$$\alpha_e = \frac{(\alpha EA)_{girder} + (\alpha EA)_{deck}}{(EA)_{girder} + (EA)_{deck}} \qquad (14)$$

The end movements, determined from Case 1 for maximum expansion and maximum contraction, are recommended for use in determining a design range of abutment movements. The larger of these two movements should be used for comparison with the limiting pile displacement, Δ, when designing abutment piles.

The end movements, $\Delta\ell$, determined from Case 2 for maximum re-expansion from a starting point of full contraction, should be used to determine passive soil pressure on the abutment. In addition, the end movements determined for Case 1 and Case 2 should be used to obtain the forces on the abutment piles to be used in designing the connection between the piles and footing. Note that the pile may not yield under the initial expansion from Case 1, which is typically a smaller movement, but may do so with Case 1 contraction or the re-expansion from Case 2. It should also be noted that the above procedures can be used to estimate design joint movements in bridges with expansion joints.

Transverse Movement in Skewed Bridges

A skewed bridge is a bridge with the longitudinal axis at an angle other than 90° with the piers and abutments. With skewed bridges, the soil passive pressure developed in response to thermal elongation has a component in the transverse direction as illustrated in figure 8. Within certain limits of skew, soil friction on the abutment will resist the transverse component of passive pressure. However, if the soil friction is insufficient, either significant transverse forces or significant transverse movements, depending on the transverse stiffness of the abutment, could be generated.

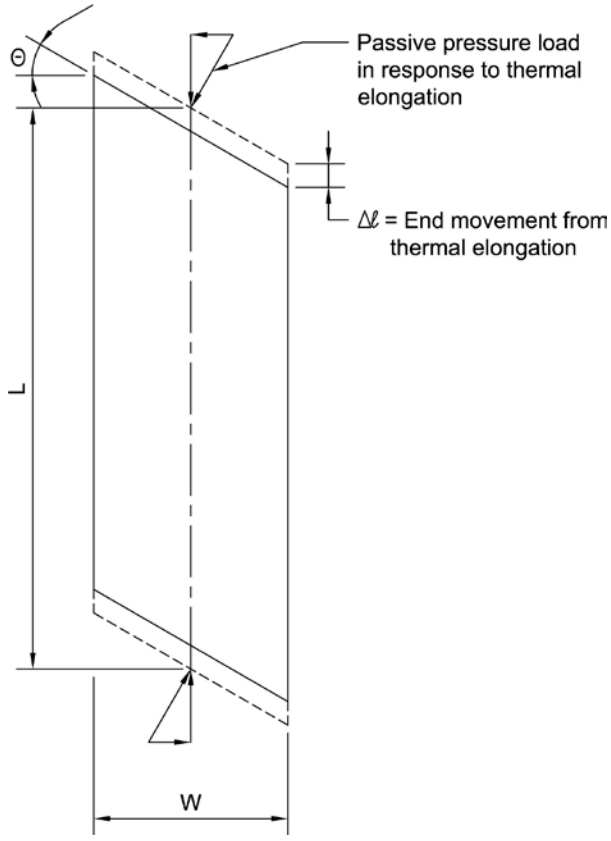

Figure 8. Components of abutment soil passive pressure response to thermal elongation in skewed bridges with integral abutments.

Because of potential problems and uncertainty related to the response of skewed integral abutments, many US State DOT's limit the skew in this type of bridge. A typical limit for the maximum skew angle for the jointless bridges used by many States is 30°. However, maximum skew angle limits in various States range from 0° to no limit.[21] There is a need to define a rational basis for limiting and/or accommodating skew angles for bridges with integral abutments. Therefore, an analytical study was carried out to investigate transverse movement in skewed bridges. This work was accomplished by developing equilibrium and compatibility equations for end abutment forces and, in the case of a typical stub abutment, solving these equations for varying skew angles and bridge length-to-width ratios.

Skew Angle Limit for Limiting Transverse Effects

Figure 9 shows the relationship between passive soil pressure response to thermal expansion and soil/abutment interface friction assuming no rotation of the superstructure.

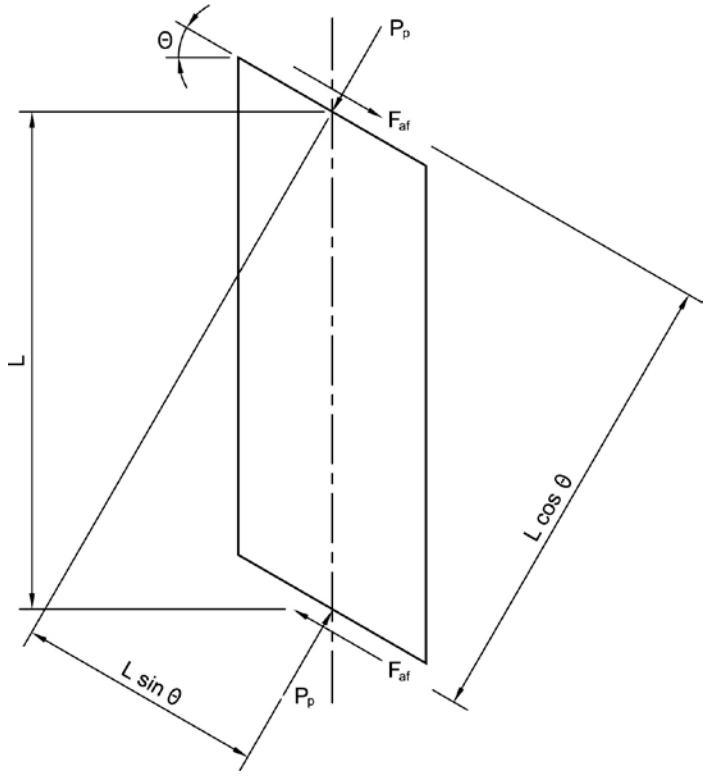

Figure 9. Soil pressure load, P_p, and soil/abutment interface friction, F_{af}.

For rotational equilibrium:

$$F_{af} (L \cos \theta) = P_p (L \sin \theta) \quad (15)$$

$$F_{af} = P_p \tan \delta \quad (16)$$

where,

P_p = Resultant normal soil pressure force
F_{aF} = Soil/abutment interface friction force
tan δ = friction factor for interface of formed concrete and soil

Substituting equation 16 into 15:

$$\tan \delta = \frac{\sin\theta}{\cos\theta} = \tan \theta$$
$$\delta = \theta \qquad (17)$$

Therefore, the bridge superstructure will be held in rotational equilibrium until the skew angle, θ, exceeds the angle of backwall friction, δ. Integral abutments are typically backfilled with granular material. NCHRP Report 343, *Manual for the Design of Bridge Foundations*, lists a friction angle of 22° to 26° for formed concrete against clean gravel, gravel sand mixtures, and well-graded rock fill with spalls.[8] Based on the data, 20° represents a reasonably conservative skew angle below which special consideration for transverse forces or transverse movement is not needed.

Forces Required to Resist Transverse Movement

With larger skew angles, the integral abutment can either be designed to resist the transverse force generated by the soil passive pressure in an attempt to keep the abutment movement predominantly longitudinal, or the abutment can be detailed to accommodate the transverse movement. Figure 10 shows the relationship for rotational equilibrium, including lateral resistance of the abutment, F_a, in addition to the wall/soil interface friction, F_{af}. For rotational equilibrium:

$$(F_a + F_{af})\,(L \cos \theta) = P_p\,(L \sin \theta) \qquad (18)$$

$$F_{af} = P_p \tan \delta$$

$$F_a = P_p\,(\tan \theta - \tan \delta) \qquad (19)$$

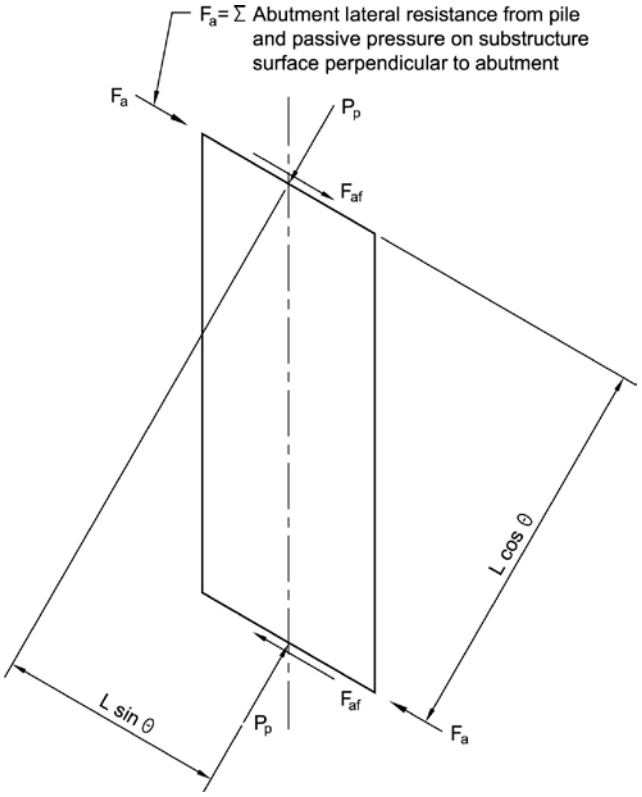

Figure 10. Abutment lateral force, F_a, required in combination with interface friction, F_{af}, for rotational equilibrium of heavily skewed bridge.

Figure 11 shows the ratio of F_a and P_p as a function of skew angle, assuming that the interface friction angle, δ, is 20°. As shown in figure11, the force required to resist transverse movement is a significant portion of the passive soil pressure response, P_p. It should be noted that P_p is not necessarily the full passive pressure response, but can be determined for the end movement using the Clough and Duncan relationships[5]. The end movement to be considered for Δ/H in figure 1 is the end movement normal to the abutment, Δ_n. This end movement is:

$$\Delta_n = \Delta \cos \theta \qquad (20)$$

where Δ is the maximum expected end movement for thermal re-expansion from the starting point of full contraction for the full range of effective bridge temperatures.

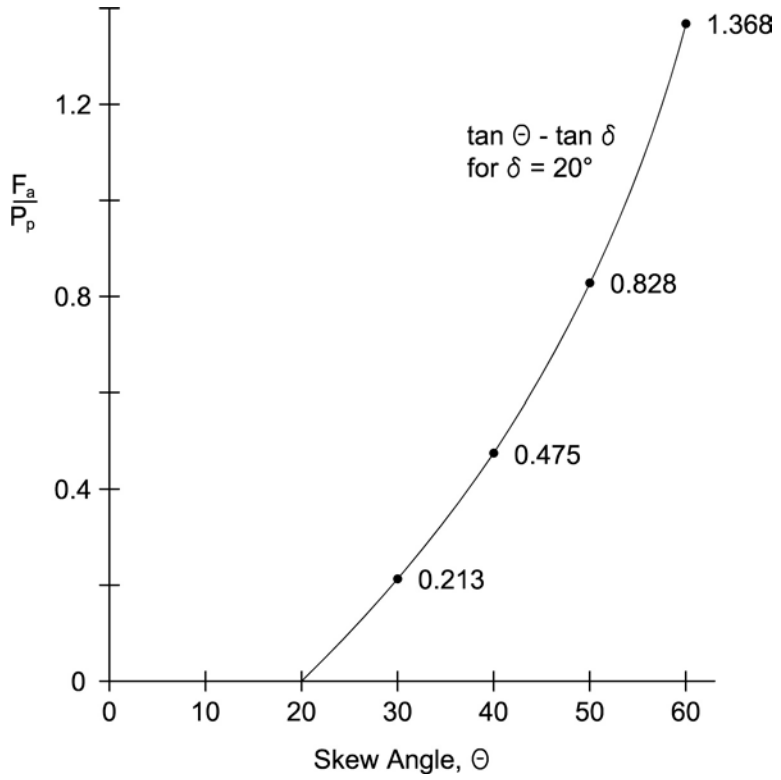

Figure 11. Relationship between force required for abutment lateral resistance, F_a, and passive pressure response, P_p, to restrain lateral movement.

For relatively short bridges in locations with small effective temperature ranges, it may be feasible to design the abutment substructure to resist F_a. It should be understood though that, for whatever means are used to develop F_a (batter pile and/or lateral passive soil resistance), lateral movements are required to develop the resistance, F_a. Therefore, details anticipating some transverse movement should be used. The expected movements are a function of the relative stiffnesses of resistance to P_p and F_a. It should also be noted that adding battered piles to an integral abutment for lateral load will also increase the stiffness in the longitudinal direction, which induces more demand on the superstructure and connections between the deck and abutments.

Expected Transverse Movement With Typical Stub Abutment

To investigate the relationship between skew angle and expected transverse movement for a typical integral stub abutment, a set of relationships were derived based on the equilibrium and compatibility of end abutment forces in the plane of the bridge superstructure. For this analysis, the superstructure is assumed to act as a rigid body with rotation, β, about the center of the deck (for a longitudinally symmetrical bridge) as illustrated in figure 12. The rotation occurs to accommodate the thermal end movement, $\Delta\ell$. Forces considered in response to this movement include soil pressure on the abutment and wingwalls, wall/soil interface friction on the abutment, and pile forces normal to and in line with the abutment and wingwalls.

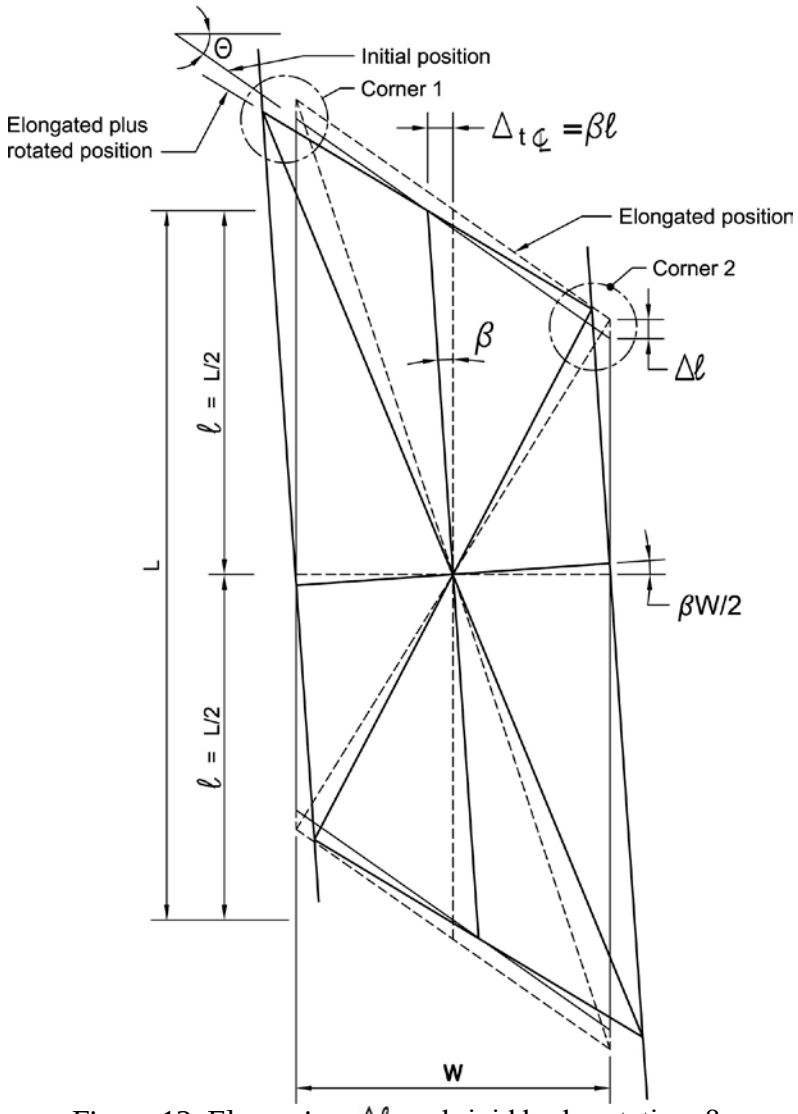

Figure 12. Elongation, $\Delta\ell$, and rigid body rotation, β.

The results in figure 13 demonstrate the increase in the transverse movement with increasing skew angle. The data in figure 13 also demonstrate the increase in transverse movement with decreasing L/W ratio. The data in figure 13 show that increasing the wingwall length relative to the abutment wall length (which includes increasing the number of wingwall piles relative to the number of abutment wall piles) can significantly decrease the transverse movement. However, the wingwalls and abutment have to be designed to transmit the restraint forces on the wingwalls into the superstructure.

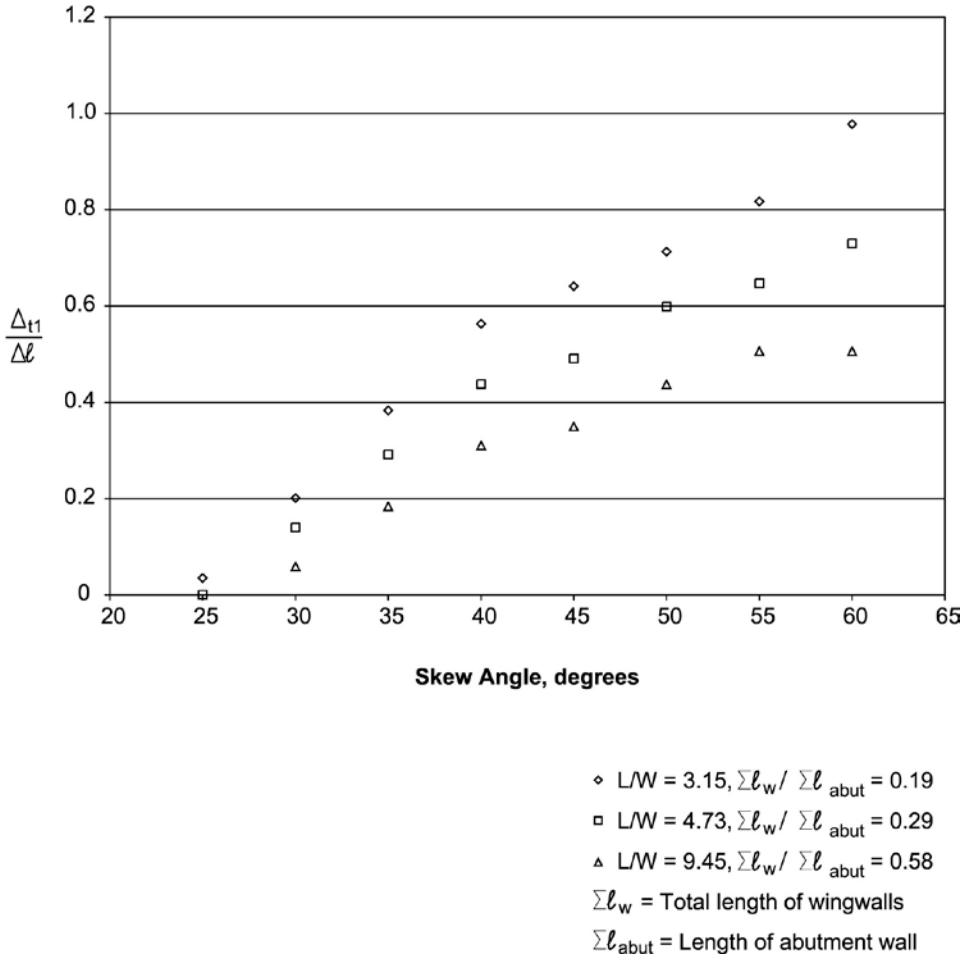

Figure 13. Relationship between transverse movement at the acute corner, Δ_{t1}, and thermal expansion, $\Delta\ell$, for an expansion of 25.4 mm (1 inch) with constant-length bridge, L = 126.77 m (415.92 ft), and varying L/W.

Figure 14 shows the resulting total longitudinal restraint force for these analyses and demonstrates the decrease in longitudinal restraint with increasing skew angle. For the full-width bridge with a L/W ratio = 3.15, the longitudinal restraint at a skew angle of 60° is approximately 60 percent of the longitudinal restraint at θ = 25°. For the larger L/W ratio = 9.45, the ratio of the longitudinal restraint at θ = 60° is approximately 70 percent of the restraint at θ = 25°. This demonstrates the increase in restraint resulting from the increase in the resistance to lateral moment caused by the larger ratio of wingwall length to abutment length.

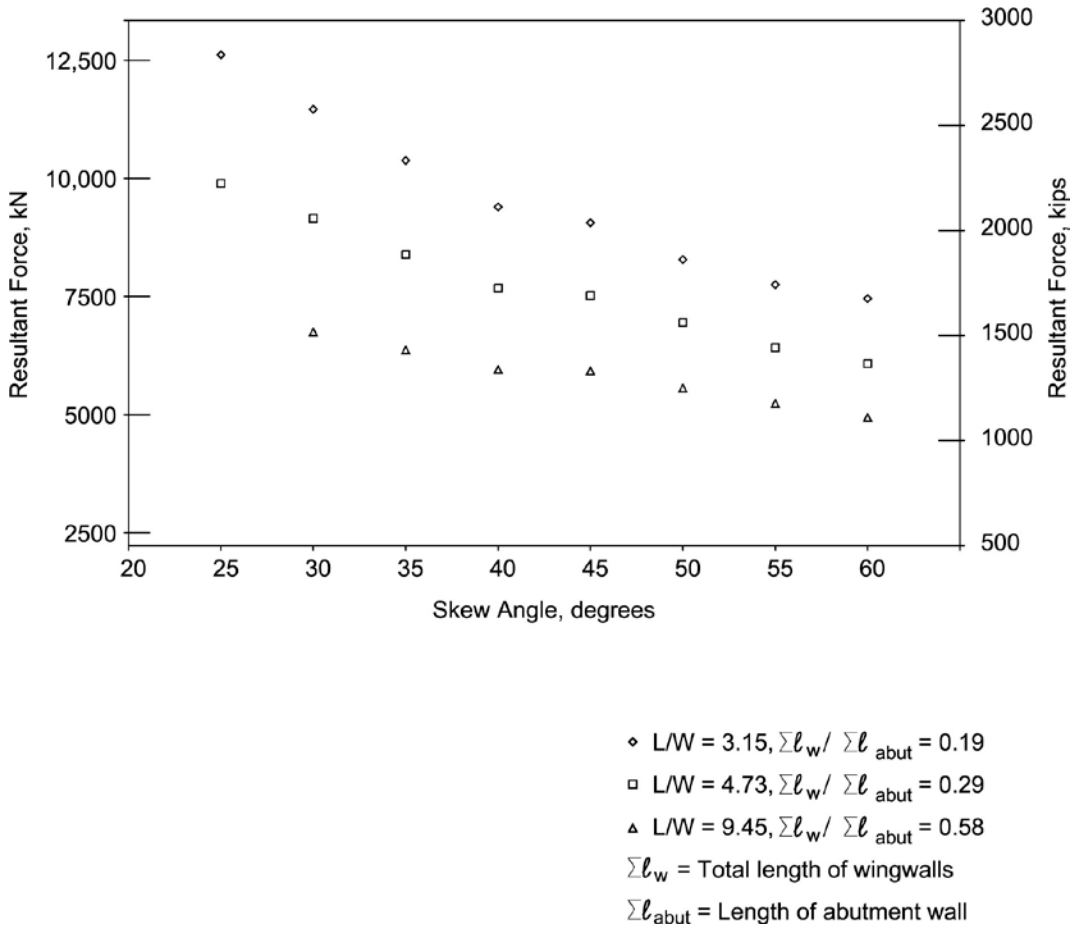

Figure 14. Relationship between resultant longitudinal restraint force and skew angle for thermal expansion, $\Delta\ell$, of 25.4 mm (1 inch) with constant-length bridge, L = 126.77 m (415.92 ft), and varying L/W.

It should be noted that the transverse movement, Δ_{t1}, discussed above is the movement of the acute corner of the bridge deck related to rigid body rotation of the superstructure caused by abutment passive restraint of longitudinal thermal expansion, $\Delta\ell$. There will also be transverse thermal expansion of the abutment. This transverse thermal expansion will be limited as compared to the longitudinal expansion, because the temperature change is moderated by the fact that abutment breastwalls are exposed to ambient air temperature on one side only and the abutment is not appreciably exposed to solar radiation. Therefore, depending on the width of the bridge and the skew angle, the transverse thermal expansion may or may not add significant additional transverse movement to the abutment wingwalls. This additional transverse movement would add to Δ_{t1} and subtract somewhat from Δ_{t2}.

To detail the abutments for the transverse movement of the corners, all interfaces of the integral abutment with other components, such as approach pavement, barrier walls, pavement for slope protection, and drainage components, should be detailed to accommodate this movement. In addition, relatively flexible connections to piers should be considered in the direction parallel to the pier caps. The analyses indicated that, for right bridges, the restraint forces from the piers into the

superstructure, resulting from longitudinal expansion, have relatively minor effects. This is for movement perpendicular to the pier cap. Foundation rotation and cracking in the pier (cantilevered from the foundation) contribute to a relatively flexible pier response for this direction of movement. The foundation and pier structure stiffness will probably be more significant for movement parallel to the pier cap. Therefore, it is recommended that the connection between the bottom of the superstructure and the pier caps be flexible in this direction. (This approach, however, may not be appropriate for seismic design.) In this case, design of the diaphragms should consider the piers' restraint of the rigid body rotations that result from passive abutment restraint of longitudinal thermal expansion.

Temperature Gradient Effects

Strains within a continuous bridge cross section subjected to a nonlinear temperature gradient are a function of two components: internal restraint strains and continuity strains. Internal restraint strains result from the difference between the unrestrained free temperature strains and the actual final restrained strain profile. The final restrained strain profile is typically assumed to be linear based on one-dimensional beam theory and the Navier-Bernoulli hypothesis that initially plane sections remain plane after bending. The internal restraint strains, which occur because of restraint within the cross section, are shown graphically in figure 15. If the nonlinear temperature gradient of figure 15(b) is applied to the cross section of figure 15(a), and if each individual fiber of the cross section is allowed to move freely, the strain profile of figure 15(c) will result. However, the final strain profile is assumed to be linear, as shown in figure 15(d). The difference between the free strain profile and the final strain profile, shown by the shaded portion of figure 15(e), is the internal restraint strains.

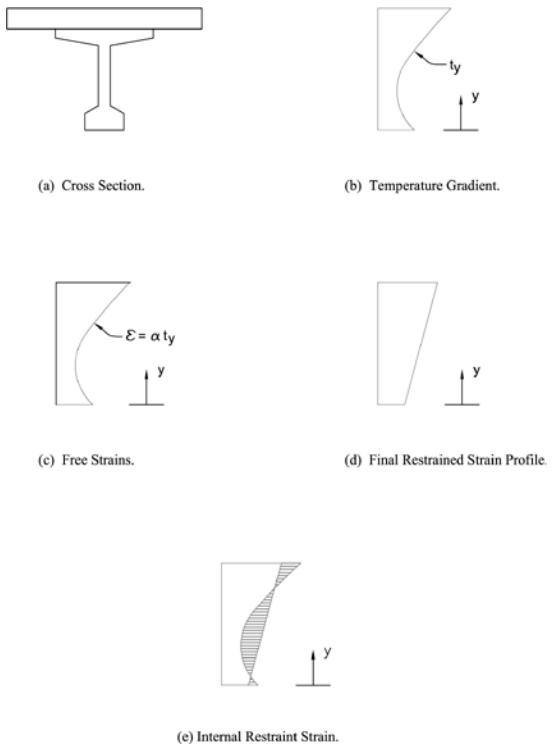

Figure 15. Diagram of restraint strains in a cross section.

These restraint strains can be calculated for a section without external axial and flexural restraints from equations developed by M.J.N. Priestley.[22] Priestley's equations for average strain and curvature, as modified for an irregular cross section, consist of the following:

$$\varepsilon_{t_{avg}} = \frac{\int \alpha_y \Delta t_y b_y E_y \, dy}{\int b_y E_y \, dy} \tag{21}$$

$$\phi = \frac{\int \alpha_y \Delta t_y b_y E_y \, y \, dy}{\int b_y E_y \, y^2 \, dy} \tag{22}$$

where,

$\varepsilon_{t_{avg}}$ = strain at the neutral axis of the cross section caused by the imposed nonlinear temperature variation along the depth and referred to as average strain in the cross section
ϕ = Curvature of the cross section due to temperature gradient
α_y = coefficient of thermal expansion as a function of depth, $\alpha_y = F(y)$
Δt_y = change in temperature of the cross section as a function of depth (the applied thermal gradient), $\Delta t_y = F(y)$
b_y = width of cross section as a function of depth, $b_y = F(y)$
E_y = modulus of elasticity as a function of depth, $E_y = F(y)$
y = distance from neutral axis of cross section

If the cross section is divided into n discrete subsections, and a transformed cross section is used through application of a modular ratio, the equations simplify to:

$$\varepsilon_{t_{avg}} = \frac{\sum_{i=1}^{n} \alpha_i \Delta t_i A_i}{A_c} \tag{23}$$

$$\phi = \frac{\sum_{i=1}^{n} \alpha_i \Delta t_i A_i y_i}{I_c} \tag{24}$$

where,

α_i = coefficient of thermal expansion in subsection i
Δt_i = change in temperature in subsection i
A_i = cross-sectional area of transformed subsection i
y_i = distance from neutral axis of cross section to subsection i

A_c = cross-sectional area of the entire composite transformed section
I_c = moment of inertia of the entire composite transformed section

The average strain and curvature are shown graphically in figure 16. The restraint strains are then calculated as the difference between the final strain profile and the free strain profile, also shown in figure 16, through application of the following equation:

$$\varepsilon_{r_y} = \varepsilon_{t_{avg}} + \phi y - \alpha_y \Delta t_y \qquad (25)$$

where,

ε_{r_y} = restraint strain as a function of depth
$\varepsilon_{t_{avg}}$ = average strain
ϕ = curvature
y = distance from neutral axis
α_y = coefficient of thermal expansion as a function of depth
Δt_y = change in temperature as a function of depth (the applied thermal gradient)

However, the above calculations assume a cross section without external axial and flexural restraints. For a simple-span bridge, the curvature resulting from the imposed thermal gradient, calculated from either equation 22 or 24, will result in a bowing of the section along the span. Only the internal restraint strains as discussed previously are present in the cross section because of the imposed nonlinear temperature variation. For a two-span continuous bridge, on the other hand, the same bowing is restrained by the center support. This external restraint gives rise to additional forces acting on the cross section. These additional forces are often referred to as secondary continuity forces since they result from the continuous nature of the structure.

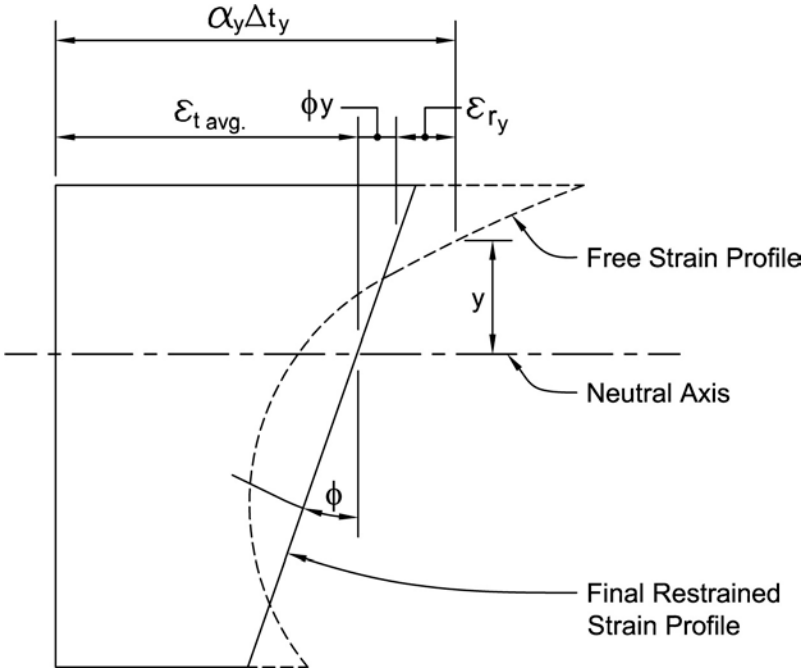

Figure 16. Restraint strain components.

The magnitude and distribution of the secondary continuity forces, and the corresponding continuity strains, are a function of the bridge cross section and the number and relative length of each span comprising the bridge. For example, the two-span bridge shown in figure 17(a) is subjected to a positive thermal gradient. The interior redundant support is removed, and the girder is allowed to bow upward as shown in figure 17(b). The curvature, ϕ, is then calculated from either equation 22 or 24, and the corresponding deflection, δ, is calculated from the second moment area theorem as $\phi L^2/8$, where L is equal to the total length of the bridge, or a+b. To restore the interior support, a force P must be applied at the location of the previously removed redundant support, which will result in a deflection equal and opposite to that caused by the initial bowing, as shown in figure 17(c). The magnitude of this force can be calculated by setting the deflection for a concentrated load at midspan of a simple-span beam equal to the curvature deflection δ, or $PL^3/48E_c I_c = \phi L^2/8$. Solving for P yields a value of $6E_c I_c \phi/L$, where E_c and I_c are the modulus of elasticity and moment of inertia, respectively, of the composite transformed section. The corresponding midspan moment (moment at the center support) is then equal to PL/4 or $(6E_c I_c \phi/L)$ L/4, which simplifies to $1.5 E_c I_c \phi$, and the complete secondary continuity moment diagram is as shown in figure 17(d).

The same approach can be used to derive secondary continuity moments for any span and support condition combination. The term $E_c I_c \phi$ is often referred to as the restraint moment, M_r, since it is the result of the internal cross-section restraint of the section when subjected to a nonlinear thermal gradient. Various span combinations will result in the secondary continuity moments ranging from a minimum of 1.0 to a maximum of 1.5 times this restraint moment. By the principle of superposition, the total thermal strains are then the combination of the internal restraint strains, as calculated from equations 21 through 25, and the continuity strains, as calculated from the one-dimensional beam theory for the continuity moments resulting from the specific support conditions of the bridge in question. Thermal stresses are then calculated directly from the thermal strains.

Positive Secondary Moments in Prestressed Concrete Beams

Positive secondary moments are affected by beam creep and differential shrinkage between the beam and the deck, positive diurnal temperature gradients, variation of the coefficient of thermal expansion between the beam and the deck, and deck heat of hydration (i.e. locked-in temperature differential between the deck and the beam).

The results of the analyses and the comparison with data from the test girder in this study indicate that accurate creep and shrinkage parameters, along with the heat of hydration effects, are necessary to reliably predict the actual continuity moments and the associated reactions. The analytical results also demonstrated the effects of cracking in relieving continuity moments and reactions; however, in doing so, the cracking induced high strains in the positive moment continuity connection (over the pier).

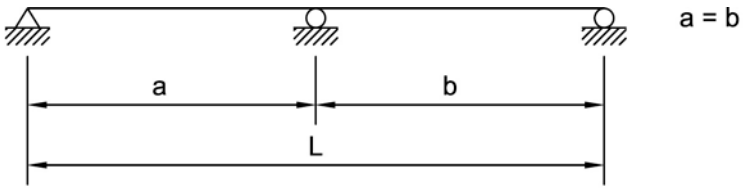

(a) Two span bridge.

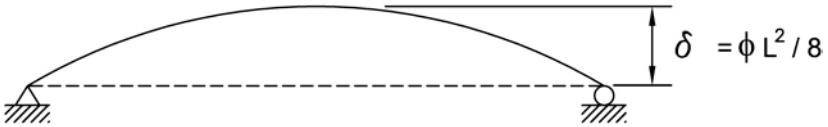

(b) Bowing after removal of redundant support.

(c) Restoration of redundant support.

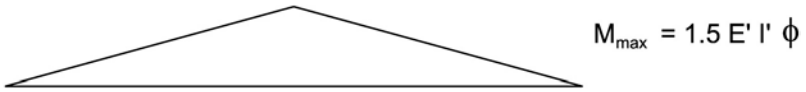

(d) Resultant secondary continuity moment diagram.

Figure 17. Two span bridge secondary continuity moments.

Observations of the test bridge indicated that positive continuity moments are significantly affected not only by creep and shrinkage in the girder and deck, but also by temperature gradients caused by daily and seasonal temperature changes, and residual stresses resulting from the heat of hydration in the deck. The level of shrinkage strain actually observed was low because of the outdoor environmental effects. Data from the test girder demonstrated that all of these factors can be additive and that the positive moment reinforcement provided in the diaphragm reached the yield stress under the combination.

Connections are made in the diaphragm and deck concrete for this type of construction so that the beams, which are simply supported for dead load, are made continuous for live load. Structural capacity for live load can be gained, particularly with the development of negative moments over the piers. However, by providing a positive moment connection, the secondary effects will probably cause positive secondary moments and cracking at the bottom of the diaphragms. The

magnitude of the positive moment that can develop depends on the amount of positive reinforcement provided and the adequacy of the anchorage of this reinforcement.

Considering the uncertainty of the factors affecting the potential for positive secondary moment, a simplified procedure to account for these effects was a prime objective. To accomplish this objective, two simplified design philosophies are proposed. The first involves eliminating the positive moment connections in the bottom of the diaphragm over the piers. This essentially eliminates positive secondary moments and the girders can be designed as simply supported for service-level stresses from dead and live loads. For ultimate strength design, as long as sufficient reinforcement is provided in the deck and a concrete diaphragm is cast between the ends of the girders so that compression exists when the crack (or control joint) closes, there will be a negative moment capacity for extreme loads. This approach eliminates the uncertainty of positive moment service-level stresses in prestressed concrete girders, but provides a jointless deck and continuous structure for strength design. The consideration of details that allow rotation to occur at the ends of the girders and to connect the piers to the superstructure are discussed below.
The second philosophy for simplifying procedures to account for positive moment effects is to design the positive moment connection to yield prior to developing stresses that could crack the prestressed beams. With this philosophy, the positive moment connection acts as a fuse to eliminate the uncertainty of the positive secondary moment effects by designing an upperbound for these effects.

ACKNOWLEDGEMENTS

This study was sponsored by the U.S. Federal Highway Administration. The support of FHWA is greatly appreciated. A large number of other researchers participated in this effort. These include T.M. Refai, T.J. Lawson, J.S. Volz, and A. Scanlon.

REFERENCES

1. Abendroth, R.E.; Greimann, L.F.; and Ebner, P.E., "Abutment Pile Design for Jointless Bridges," *Journal of Structural Engineering*, ASCE Vol. 115, No. 11, 1989, pp. 2914-2929.

2. TRB, *Bridge Deck Joint-Sealing Systems, Evaluation and Performance Specification*, NCHRP Report 204, National Research Council, Washington, DC, 1979.

3. Emerson, M., *Bridge Temperatures Estimated From the Shade Temperature*, TRRL Laboratory Report 696, TRRL, Crowthorne, Berkshire, Great Britain, 1976, 54 pp.

4. Imbsen, R.A., et al., *Thermal Effects in Concrete Bridge Superstructures*, NCHRP Report 276, TRB, Washington, DC, September 1985, 99 pp.

5. Clough, G.W., and Duncan, J.M., "Earth Pressures," *Foundation Engineering Handbook*, Second Edition, Edited by H.Y. Fung, Van Nostrand Reinhold, New York, NY, 1991, pp. 223-235.

6. Tabatabai, H.; Oesterle, R.G., and Lawson, T.J., *Jointless Bridges, Experimental Research and Field Studies*, Volume I, Final Report to FHWA, August 2005, 972 pp.

7. Oesterle, R.G.; Refai, T.M.; Volz, J.S.; Scanlon, A.; and Weiss, W.J., *Jointless Bridges, Analytical Research and Proposed Design Procedures*, Volume II, Final Report to FHWA, February 2005.

8. Barker, R.M.; Duncan, J.M.; Rojiani, K.B.; Ooi, P.S.K.; Tan, C.K.; and Kim, S.G., *Manual for the Design of Bridge Foundations*, NCHRP Report 343, Transportation Research Board (TRB), Washington, DC, December 1991, 308 pp.

9. Schaefer, V.R., and Koch, J.C., *Void Development Under Bridge Approaches*, Report No. SD90-03, South Dakota State University, Brookings, SD, November 1992, 147 pp.

10. AASHTO, *Standard Specifications for Highway Bridges*, 14th Edition, Washington, DC, 1989, 420 pp.

11. Shams, M., and Saadeghvaziri, M.A., "State of the Art of Concrete-Filled Steel Tubular Columns," *ACI Structural Journal*, ACI, September-October 1997, pp. 558-571.

12. Zederbaum, J., "Factors Influencing the Longitudinal Movement of Concrete Bridge System With Special Reference to Deck Contraction," *Concrete Bridge Design*, ACI Publication No. SP-23, ACI, Detroit, MI, 1969, pp. 75-95.

13. Witecki, A.A. and Raina, V.K., "Distribution of Longitudinal Horizontal Forces Among Bridge Supports," *Concrete Bridge Design*, ACI Publication SP-23, ACI, Detroit, MI, 1969, pp. 803-815.

14. ASHRAE, *Fundamentals Handbook*, ACI, New York, NY, 1993.

15. AASHTO, *AASHTO LRFD Bridge Design Specifications*, 5th Edition, Washington, DC, 2010.

16. Technical Report No. 65, *Expansion Joints in Buildings***,** National Academy of Science, 1979.

17. ACI Committee 209, *Prediction of Creep, Shrinkage, and Temperature Effects in Concrete Structures*, Report No. ACI 209R-92, ACI, Detroit, MI, 1992, 47 pp.

18. Kosmatka, S.H., and Panarese, W.C., "Chapter 13, Volume Changes in Concrete," *Design and Control of Control Mixtures*, 13th Edition, Portland Cement Association (PCA), Skokie, IL, 1988, pp. 151-162.

19. Bazant, Z.P., and Panula, L., "Creep and Shrinkage Characterization for Analyzing Prestressed Concrete Structures," *PCI Journal*, May/June 1980, pp. 86-121.

20. Emanuel, J.H., and Hulsey, J.L., "Prediction of the Thermal Coefficient of Expansion of Concrete," *Journal of American Concrete Institute*, Vol. 74, No. 4, April 1977, pp. 149-155.

21. Chandra, V., et al., *Draft Report on Precast Prestressed Concrete Integral Bridges, State-of-the-Art*, Precast/Prestressed Concrete Institute, 1995, 113 pp.

22. Priestley, M.J.N., "Design of Concrete Bridges for Temperature Gradients," *ACI Journal*, ACI, No. 5, May 1978, pp. 209-217.